Determination and Comparison of Rotational Velocity in a Pseudo 2-D Fluidized Bed Using Magnetic Particle Tracking and Discrete Particle Modeling

K. A. Buist, T. W. van Erdewijk, N. G. Deen, and J. A. M. Kuipers
Department of Chemical Engineering and Chemistry, Multiphase Reactors Group,
Eindhoven University of Technology, 5600 MB Eindhoven, The Netherlands

DOI 10.1002/aic.14949
Published online July 24, 2015 in Wiley Online Library (wileyonlinelibrary.com)

Modeling of dense granular flow has been subject to a large amount of research. Particularly discrete particle modeling has been of great importance because of the ability to describe the strongly coupled dynamics of the fluid and the solids in dense suspensions. Many studies have been reported on the validation of the translational particle velocities predicted by using these models. The rotational motion however has received far less attention, mainly because of the spherical nature of the particles under investigation and the lack of techniques with the capability to study the rotational behavior of the solid phase. In this study, we will for the first time present experimental data on the rotational behavior of particles in a pseudo two-dimensional fluidized bed setup using Magnetic Particle Tracking. In addition the experimental results are compared to data obtained from discrete particle simulations. © 2015 American Institute of Chemical Engineers *AIChE J*, 61: 3198–3207, 2015

Keywords: fluidization, noninvasive monitoring, magnetic particle tracking, rotational velocity, discrete particle modeling

Introduction

In many industries, fluid–solid interactions are of great importance, for instance, in drying, granulation or pelletization, combustion, and food processing. Often the solids phase is nonideal and composed of nonspherical particles. This makes accurate prediction of the solids motion using CFD modeling difficult. Particularly, the effect of the relative orientation of the particle to the flow direction on the drag and lift is difficult to assess. Second, lack of experimental data on the orientation and rotational behavior makes validation difficult if not impossible. In this article, we will discuss, for ideal spherical particles, the rotational behavior and orientation in a pseudo two-dimensional (2-D) fluidized bed based on experimental data obtained with a Magnetic Particle Tracking (MPT) technique. We will also compare the results with data obtained from a Discrete Particle Model (DPM).

Attempts at studying the rotational behavior of solids in granular flow have been made with moderate success. Using particle tracking velocimetry Wu et al.[1] have been able to study rotation of 500 μm particles in a circulating fluidized bed. Phillips et al.[2] have used Laser Doppler Anemometry to study the rotation of 150 μm oil particles. However, these techniques are restricted to use in systems with optical access. Yang et al.[3] have used a multi Positron Emission Particle Tracking technique to study the motion of 12 mm cubes in a rotating can. By embedding 3 markers in the cube the relative orientation could be determined. The technique is based on correlating the trajectories of the back-to-back gamma rays. By removing the trajectories of the strongest tracer the position of the second and third tracer could be determined. Unfortunately, the minimum relative distance between the tracers is limited to 5 mm. Yang et al.[3] have been able to determine translational and rotational motion of 12 mm cubes at 40 Hz with 6 mm standard deviation errors, with translation and rotational velocities up to 0.5 m/s and 50 rpm.

MPT on the other hand is by its nature capable of determining the orientation with no need to modify the tracer particles either by adding markers or applying a pattern on the particle surface. The position and orientation of the magnet induces a distinct magnetic field (Buist et al.[4]). This allows the use tracer particles in the order of a few millimeters in size. Neuwirth et al.[5] have shown the capability of determining the translational and rotational velocity of 6 mm spheres in a rotor granulator. In their study, they compared the results with a discrete element method, and found a good comparison for the spread in rotational velocities in the rotor granulator.

In the DPM, the particle translation and rotation are described by Newton's second law of motion. So far, mostly the translation was studied, as this is the dominant factor in describing the particle dynamics. Questions have arisen whether rotation has any influence at all.[6] Van Buijtenen et al.[7] found that the near wall translational velocity predicted by the DPM does not match well with experiments for the case of a spout-fluidized bed. They thought this was a problem related to the friction and increased the particle-wall friction for the whole system. Goniva et al.[8] opt for a different

Correspondence concerning this article should be addressed to N. G. Deen at N.G.Deen@tue.nl.

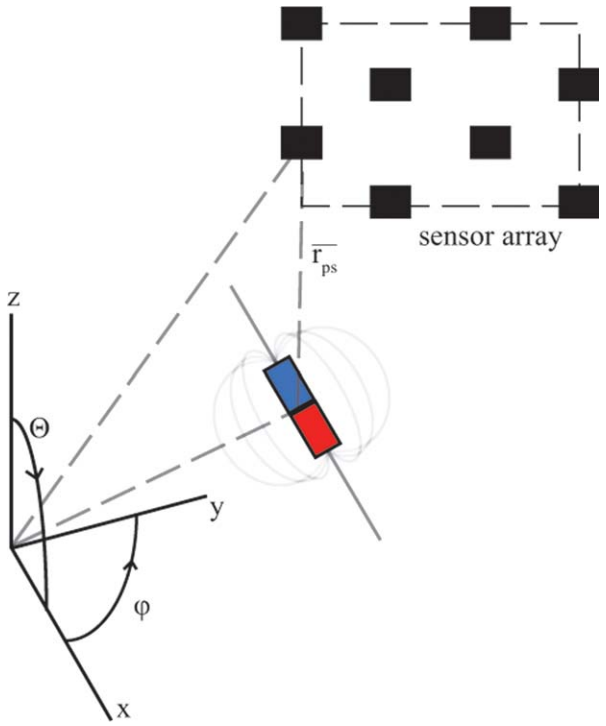

Figure 1. Schematic representation of the principle behind MPT.

[Color figure can be viewed in the online issue, which is available at wileyonlinelibrary.com.]

explanation and implemented a model to describe rotational friction. Both studies reveal that changing either one of the parameters increases the accuracy in the translation of the DPM for a pseudo 2-D setup. However, the most noticeable effect should be in the rotational behavior which was not directly studied, due to lack of experimental data. With the addition of information on the rotation of particles in granular flows it is possible to look at the completeness of the DPM and more specifically on the role of the different frictional forces.

This article is organized as follows. In the methods section we will discuss the MPT technique and the DPM. In the section experimental setup we will discuss the pseudo 2-D fluidized bed, the sensor array and the Helmholtz coil. Thereafter, the results will be presented and conclusions will be summarized.

Methods

Magnetic particle tracking

The principle of the MPT technique has been thoroughly discussed by Buist et al.[4] We will give a short summary here. A schematic representation of the technique is given in Figure 1. A magnetic tracer particle is added to the fluidized bed. This magnetic tracer particle will induce a quasistatic magnetic field at the sensor given by Eq. 1

$$\bar{H}(\bar{e}_p, \bar{r}_{ps}) = \frac{1}{4\pi}\left(-\frac{\mu_m \bar{e}_p}{|\bar{r}_{ps}|^3} + \frac{3\mu_m(\bar{e}_p \cdot \bar{r}_{ps})\bar{r}_{ps}}{|\bar{r}_{ps}|^5}\right) \quad (1)$$

where $\bar{r}_{ps} = \bar{r}_p - \bar{r}_s$ is the relative distance of the tracer particle to the sensor, μ_m is the magnetic moment of the tracer particle, and $\bar{e}_p$ is the orientation unit vector of the magnet, calculated via a transformation of the angles; ϕ and θ from the spherical to the Cartesian coordinate system. Equation 1 gives the magnetic field. However, to obtain an estimate of the sensor output S_t the magnetic field $\bar{H}$ has to be multiplied with the orientation of the sensor ($\bar{e}_s$) in this field

$$S_t = \bar{H}(\bar{e}_p, \bar{r}_{ps}) \cdot \bar{e}_s \quad (2)$$

Evaluation of this field at the sensor positions will result in an estimate of the position and orientation. By comparing the result of the theoretical magnetic field strength at the sensor with the measured value, the most probable position and orientation can be determined. This is an inverse problem with 5 degrees of freedom that can be solved by minimizing the following quantity

$$Q = \sum_{i=1}^{72} \frac{((S_{m,i} - \langle S_m \rangle) - (S_{t,i} - \langle S_t \rangle))^2}{\Delta S_{m,i}{}^2} \quad (3)$$

The quality function (3) is corrected for the standard deviation in each individual sensor signal ($\frac{1}{\Delta S_{m,i}{}^2}$), this ensures that less accurate sensors have less influence on the quality function. Second, the quality function is corrected for stray fields using a gradiometer ($\langle S \rangle$). Equation 3 is a function that is bounded between zero and infinity. To increase the accuracy and simplicity of the minimization function, we applied a function that calculates the probability of finding a tracer particle at position x, y, z with orientation ϕ, θ from the mean value of a sensor and the standard deviation of the sensor data, following

$$P = \frac{\sum_{i=1}^{72}\left(\mathrm{erf}\left(\frac{S_{m,i} - S_{t,i}}{\sigma_{S_{m,i}}}\right)\right)}{N} \quad (4)$$

Equation 4 signifies the average of all the probabilities of finding $S_{t,i}$ given $S_{m,i}$ and $\sigma_{S_{m,i}}$. The main advantage of Eq. 4 over Eq. 3 is that determining the probability allows for a minimization function bound between 0 and 1 instead of 0 and infinity and directly relates the quality of the determined position and orientation in terms of the standard deviation or noise in the signal.

Using sequential quadratic programming (SQP) as the minimization algorithm, the most likely position and orientation of the tracer particle can be determined. With the SQP method constraints to the solution can be set. For the pseudo 2-D setup the following constraints have been set, slightly outside the physical domain to allow for error margins

$$\begin{aligned} 0 - \Delta x \le \frac{x}{W} \le 1 + \Delta x \\ 0 - \Delta y \le \frac{y}{D} \le 1 + \Delta y \\ 0 - \Delta z \le \frac{z}{H} \le 1 + \Delta z \end{aligned} \quad (5)$$

For the orientation, formal constraints can be set for the unit vector. By adding a constraint for the norm of the vector the total degrees of freedom remain five (x,y,z,ϕ,θ)

$$\begin{aligned} |\bar{e}_p| &= 1 \\ -1 \le e_x \le 1 \\ -1 \le e_y \le 1 \\ -1 \le e_z \le 1 \end{aligned} \quad (6)$$

Discrete particle modeling

In the DPM, the gas phase is described by the volume-averaged Navier–Stokes equations[9]

$$\frac{\partial}{\partial t}(\varepsilon_f \rho_f)+\nabla\cdot(\varepsilon_f \rho_f \bar{u})=0 \tag{7}$$

$$\frac{\partial}{\partial t}(\varepsilon_f \rho_f \bar{u})+\nabla\cdot(\varepsilon_f \rho_f \bar{u}\bar{u})=-\varepsilon_f \nabla p-\nabla\cdot(\varepsilon_f \bar{\bar{\tau}}_f)+\bar{S}_p+\varepsilon_f \rho_f \bar{g} \tag{8}$$

With S_p a source term for the momentum exchange between particles and the gas

$$S_p=\sum \frac{\beta V_p}{1-\varepsilon_f}(\bar{v}_p-\bar{u})\delta(\bar{r}-\bar{r}_p) \tag{9}$$

The drag coefficient, β, is calculated using the Ergun[10] and Wen and Yu[11] equations

$$\begin{aligned} F&=\frac{\beta d_p^2}{\mu}=150\frac{(1-\varepsilon_f)^2}{\varepsilon_f}+1.75(1-\varepsilon_f)\mathrm{Re}_p \\ F&=\frac{\beta d_p^2}{\mu}=\frac{3}{4}C_D\mathrm{Re}_p(1-\varepsilon_f)\varepsilon_f^{-2.65}, \\ C_D&=\max\left(\frac{24}{\mathrm{Re}_p}\left(1+0.15\mathrm{Re}_p^{0.687}\right),0.44\right) \\ \mathrm{Re}_p&=\frac{\epsilon_f \rho_f|\bar{u}-\bar{v}_p|d_p}{\mu_f} \end{aligned} \tag{10}$$

The particle phase is described using Newton's equations

$$m_p\frac{d^2\bar{r}_p}{dt^2}=-V_p\nabla p+\frac{\beta V_p}{1-\varepsilon_f}(\bar{u}-\bar{v}_p)+m_p\bar{g}+\sum \bar{F}_{ab} \tag{11}$$

$$I_p\frac{d^2\bar{\theta}_p}{dt^2}=\bar{T}_p+\bar{T}_h \tag{12}$$

The forces in Eqs. 11 and 12 represent the far field pressure force, the drag force, the gravity force and the contact forces. $\bar{r}_p$ is the particle position, $\bar{\theta}_p$ is the orientation I_p is the inertia, $\bar{T}_p$ the torque due to collisions, and $\bar{T}_h$ the hydrodynamic torque. The particle contact model is adopted from Cundall and Strack[12]

$$\bar{F}_{ab,n}=-k_n\delta_n\bar{n}_{ab}-\eta_n\bar{v}_{ab,n} \tag{13}$$

$$\bar{F}_{ab,t}=\min\left(-k_t\delta_t\bar{t}_{ab}-\eta_t\bar{v}_{ab,t},-\mu_{fr}|\bar{F}_{ab,n}|\bar{t}_{ab}\right) \tag{14}$$

$$\bar{T}_p=R_a\bar{n}_{ab}\bar{F}_{ab,t} \tag{15}$$

The normal and tangential spring stiffness for each of the particle sizes are chosen such that under the given conditions the maximum particle overlap is always less than 1% of the particle diameter, for a maximum relative velocity of 1 m/s. For a more complete overview, the authors refer to Deen et al.[9] Table 1 gives an overview of the parameters used in the simulations.

Table 1. Overview of Simulation Parameters

System Properties			Particle Properties		
Width	0.3	m	d_p	3.0	mm
Depth	0.015	m	ρ_f	1.2	kg/m^3
Height	1.0	m	μ_f	$1.8\cdot10^{-5}$	kg/ms
Nx	30		ρ_p	2600	kg/m^3
Ny	2		k_n	12,000 N/m	
Nz	100		k_t	2800 N/m	
			e_n	0.97	
			e_t	0.33	
			$\mu_{fr,p\text{-}p}$	0.10	
			$\mu_{fr,p\text{-}w}$	0.30	
			$\mu_{fr,r}$	0.125	

Hydrodynamic torque

The DPM described in the previous section does not contain a coupling between the rotation of the particle and the fluid phase. In literature, this coupling has consistently been neglected as it is expected to have a negligible effect. In this section, the validity of this assumption is checked. For the determination of the translation of particles following the force balance of Eq. 11, there is a similar coupling between the fluid and the particle rotation. So far, in the DPM this was neglected and rightfully so, as the magnitude of this force, especially for gasses, seems small. However, when taking into account the effect the dense packing has on the drag force, the magnitude of this hydrodynamical torque may become large enough to have an influence on the rotational behavior. Dennis et al.[13] gave a correlation for the hydrodynamic torque for a single sphere in a flow in the dilute limit, following the work of Sawatzki[14]

$$T_h=C_r\frac{1}{2}\rho_f r^5|\bar{\Omega}|\bar{\Omega} \tag{16}$$

$$C_r=\frac{32}{\mathrm{Re}_r}(1+0.2\mathrm{Re}_r) \tag{17}$$

with Re_r

$$\mathrm{Re}_r=\frac{\varepsilon_f \rho_f|\bar{\Omega}|d_p^2}{\mu_f} \tag{18}$$

With $\bar{\Omega}=\frac{1}{2}\nabla\times\bar{u}-\bar{\omega}$ and $\varepsilon_f=1$. One can notice the great similarity with the Schiller and Naumann[15] equation. By adding a Richardson and Zaki[16] correction, we can account for the presence of neighboring particles and hence change Eq. 16 such that it is applicable for different solid fractions $\varepsilon_f\neq1$ and thus for use in fluidized beds

$$\bar{T}_h=\varepsilon^{-2.65}\frac{32}{\mathrm{Re}_r}(1+0.2\mathrm{Re}_r)0.5\rho_f r^5|\bar{\Omega}|\bar{\Omega} \tag{19}$$

The Richardson and Zaki[16] correction is a necessary ad hoc assumption and the proper way of testing its validity would be the use of Direct Numerical Simulations, which is beyond the scope of this work. Simulations have been run with and without the hydrodynamic torque. The profiles and values of the rotational velocity did not change significantly. The magnitude of the collisional and hydrodynamic torque differed by 3–4 orders. Even though the hydrodynamic torque is a constant force and the collisional torque acts periodically, it is not enough to dampen the collisional behavior. Note that for nonspherical particles the effect of hydrodynamic torque might become important, because the effect of hydrodynamic torque increases by two orders of magnitude Zastawny et al.[17] For nonspherical particles and or small particles the Magnus and Safmann forces also have to be taken into account. A similar approach as in Eqs. 16–19 can be used to apply these lift forces. A parametric study using for instance DNS can be used to check the validity of applying a Richerdson and Zaki correction.

Rolling friction

In studying the behavior of particles in a spout-fluidized bed, which is very similar to our system, Goniva et al.[8] incorporated a rolling friction model

Figure 2. MPT sensor array and pseudo 2-D fluidized bed setup.

[Color figure can be viewed in the online issue, which is available at wileyonlinelibrary.com.]

$$\bar{T}_{\mathrm{p,r}} = R_{\mathrm{p},\mu} k_{\mathrm{p,n}} \Delta\bar{x}_{\mathrm{p}} \frac{\bar{\omega}_{\mathrm{p,rel}}}{|\bar{\omega}_{\mathrm{p,rel}}|} r_{\mathrm{p}} \tag{20}$$

The authors mention that adding a rolling friction model like Eq. 20 with a friction parameter of 0.125 gave the best results in describing the translational velocity near the wall. In the model described above a similar rolling frictional model was incorporated

$$\bar{T}_{\mathrm{p,r}} = \mu_{\mathrm{rfr}} |\bar{F}_{\mathrm{n}}| \bar{t}_{\mathrm{ab}} \tag{21}$$

In essence adding a rolling friction model like Eqs. 20 or 21 means lowering the frictional limit allowing for less rotation. As both the particle-particle and particle-wall friction parameter are already 0.1, addition of a rolling friction of the same order of magnitude would cancel rotation totally we decided to not use the rolling friction model. The addition of a rolling friction thus has the same effect as lowering the friction coefficient. The friction coefficient is thus a lump sum of different frictional effects limiting the rotational behavior of particles.

Experimental Setup

For this study, a pseudo 2-D fluidized bed setup was used, the same as in Buist et al.[4] This setup is also very suitable to compare with the DPM because of its limited size.

In Figure 2, a picture of the pseudo 2-D fluidized bed is shown. The dimensions of the bed are 0.30 by 0.015 by 1.0 m (width, depth, and height). The bottom of the bed consists of a distribution chamber topped with a porous distributor plate with a pore size of 10 μm. All parts of the setup are made of aluminum or nonmagnetic stainless steel. The sensor array, consisting of 6 rows of 4 tri-axis AMR-sensors, is placed directly in front of the setup. Setup and control are courtesy of Matesy GmbH. This leads to a total of 72 sensors capable of operating at 1 kHz. Width and height of the sensor array is 0.35 by 0.65 m. An overview of all settings and properties is given in Table 2.

As a first test the error in the orientation as a function of the magnetic moment and the distance between the tracer particle and the nearest sensor is studied. Two magnets with magnetic moment 0.031 and 0.181 Am^2 was placed at fixed positions from the radius of the three-dimensional sensor array. Second 5 magnets with differing size and magnetic moment were placed in the center of the sensor array. The error in the determination of the errors is shown in Figure 3. It can be seen that the error increases linearly with decreasing magnet strength while the error increases linearly with increasing relative distance, as can be expected based on Eq. 1. Except for the magnet with a magnetic moment of 0.181, the error seems constant which is probably due to the large strength of the magnet. Similar results have also been found for the translational behavior in Buist et al.[4]

As a second test the particle is fluidized and the distribution in orientation angle is studied. Figure 4 shows both the ideal and actual spread of the azimuthal and inclination angles. The ideal shape is governed by a uniform distribution for the azimuthal angle and $\sin\theta$ for the inclination angle. From Figure 4, it can be seen that there is a deviation between the ideal and actual orientation distributions. There is a slight preferred angle of $\phi = -60^{\circ}$ and $\theta = 140^{\circ}$, which relative to the sensor and setup orientation appeared to be an alignment with the earth's magnetic field; pointing North and downwards. In other words: the magnetic marker acts as a compass, which could have been expected. This is unwanted especially when in a later stage nonspherical particles will be studied, where preferred angles due to its shape are studied. To cancel the

Table 2. Settings and Parameters of the Experimental Setup

Fluidized Bed	
Width	0.3 m
Height	1.0 m
Depth	0.015 m
Porous plate	3 mm thick
Average pore size	10 μm
Mass flow controller (max capacity)	1200 L/min
Material front plate	glass
Other materials	aluminum and stainless steel (nonmagnetic)
MPT Sensor Array	
Sensor type	tri-axis AMR
Amount	3 * 24
Frequency	1000 Hz
Dimensions	0.35, 0.65 m (width, height)
Particles	
Bed material size	3.0 mm
Density	2526 kg/m^3
Minimum fluidization velocity	1.55 m/s
Magnetic marker size	4.7 mm
Density	2100 kg/m^3
Magnetic moment	0.0125 Am^2
Minimum fluidization velocity	1.7 m/s

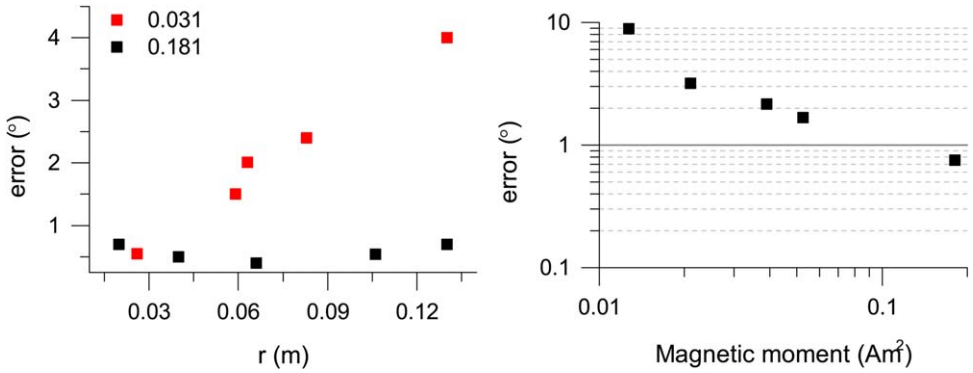

Figure 3. Effect of relative distance(left) and magnetic moment(right) on the error in the determination of the angles.

[Color figure can be viewed in the online issue, which is available at wileyonlinelibrary.com.]

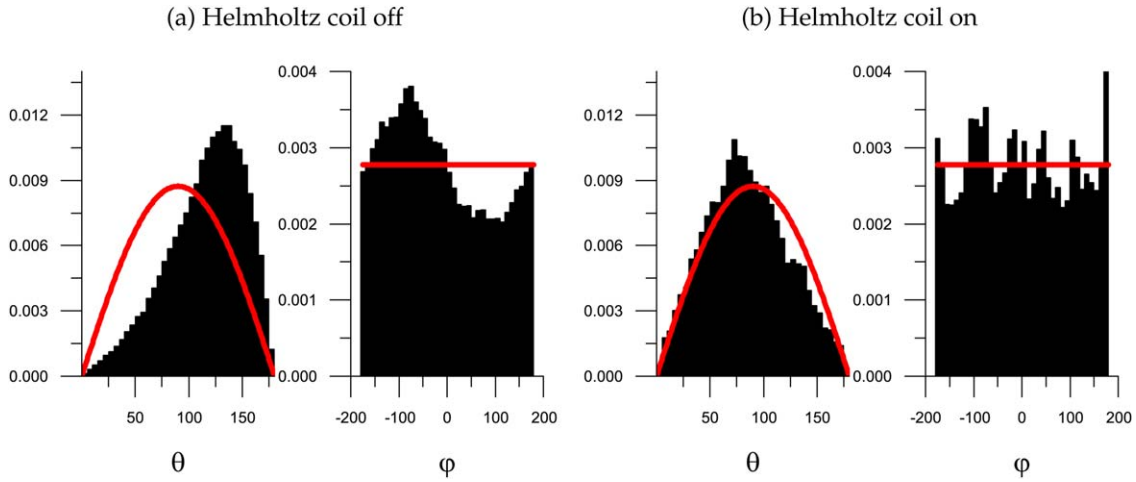

Figure 4. Histogram of the angle distributions with the Helmholtz coil off (a) and on (b).

[Color figure can be viewed in the online issue, which is available at wileyonlinelibrary.com.]

effect of the earth's magnetic field on the particle orientation a Helmholtz coil was installed.

The Helmholtz coil is a set of two square rings of 2 meter in diameter, 1 m in height apart. A schematic picture is provided in Figure 5. The orientation has to be set opposite to the earth's magnetic field and the current through the coil has to be set such that the strength of the field equals the earth's magnetic field, following Biot-Savart's law. The two fields will oppose each other, cancelling each other out. This will allow the tracer particle to orientate freely. The size of the magnetic free zone follows from the Biot-Savart law leading to 0.5 m in diameter and height.

The experiment in the previous section was repeated to see whether the influence of the earth's magnetic field was cancelled and the Helmholtz coil was operating properly.

Figure 4 shows the results of the angle distributions of a fluidization experiment with and without an operational Helmholtz coil. When the earth's magnetic field is cancelled by the Helmholtz coil the distribution of the angles shows a nice close-to-ideal behavior. There is some remaining noise that is related to the limited number of data points.

Results

To make a proper comparison between the results from the MPT and the DPM three phenomena are checked: (1) the occupancy to show that the particles have the same distribution inside the pseudo 2-D system, (2) the translation via a quantitative comparison of the vertical velocity component at different cross-sections of the bed, and (3) a qualitative and

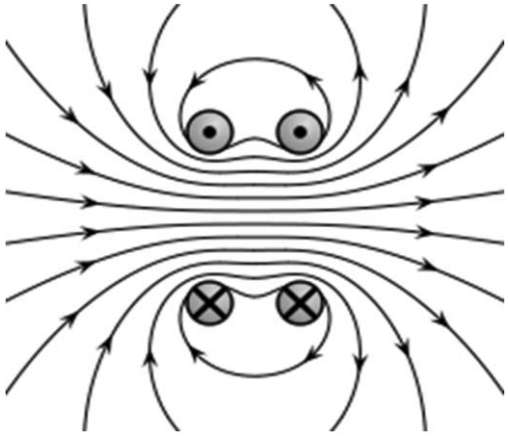

Figure 5. Schematic of a Helmholtz coil, depicting the current loop, with current coming out from the surface at the dots, and entering the surface at the crosses.

The field lines run from left to right.

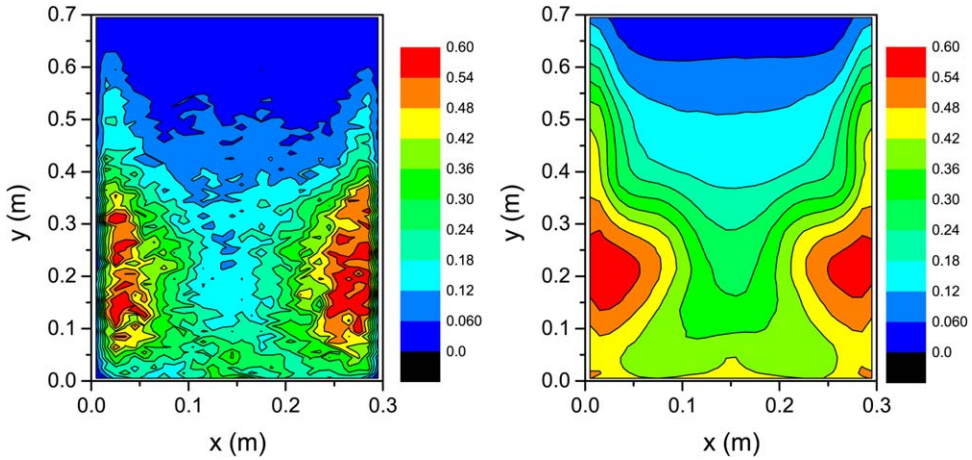

Figure 6. Mean bed solids fraction of the magnet (left) in the MPT and tracer particles (right) in the DPM, $u_0 = 3.5$ m/s.

[Color figure can be viewed in the online issue, which is available at wileyonlinelibrary.com.]

quantitative comparison of the rotational velocity of the magnetic marker and a representative tracer particle in the DPM. The experiments have been performed with a superficial velocity of 3.5 and 2.5 m/s at a sampling rate of 50 Hz.

The relevant parameters of the experiment and simulation are given in Tables 1 and 2. Because the magnetic tracer particle has different properties then the bulk material, 600 tracers are added to the DPM simulation. These tracers have the same size and mass as the magnetic tracer and a moment of inertia that is defined as

$$I = \int_0^{r_2} \frac{2}{3} r^2 \mathrm{d}m = \frac{8}{3} \int_0^{r_2} \pi \rho r^4 \mathrm{d}r \tag{22}$$

For the computation of I, it is important to account for the composite nature of the tracer particle with a dense core ($r < r_1, \rho_c = 7600\,\mathrm{kg/m^3}$) and a less dense shell ($r_1 < r < r_2, \rho_s = 250\,\mathrm{kg/m^3}$)

$$I = \frac{8}{15} \pi \left(\rho_c r_1^5 + \rho_s \left(r_2^5 - r_1^5 \right) \right) \tag{23}$$

Second, because the particles are quite large, we found a difference in bed expansion, especially at lower superficial velocities. We found that the reason for this is a mismatch of the minimum fluidization velocity between experiments and simulations. In the experiments, the minimum fluidization velocity is 1.55 m/s, however, with the given drag law (Ergun/Wen&Yu), the minimum fluidization velocity in the simulations is 1.45 m/s. To correct for this, we choose to keep the excess gas velocity ($u_{ex} = u_0 - u_{mf}$) the same for both the experiments and the simulations. In the simulations, therefore, we used $u_0 = 2.35$ and 3.28 m/s for the background velocity, relating to 2.5 and 3.5 m/s in the experiments.

The occupancy is a measure for how often a tracer particle passes a particular position, following

$$O(i,j) = \frac{N_{\mathrm{gridcells}}}{N_{\mathrm{meas}}} \sum_1^{N_{\mathrm{meas}}} \delta \quad \forall \delta = \begin{vmatrix} 1 & p \in (i,j) \\ 0 & p \ni (i,j) \end{vmatrix} \tag{24}$$

A value of 1 for the occupancy signifies the particle has passed that position as often as might be expected based on the average value. Occupancy values higher than 1 signify the particle has a tendency to stay at that particular position more than average. From the occupancy the solids fraction can be calculated[18]

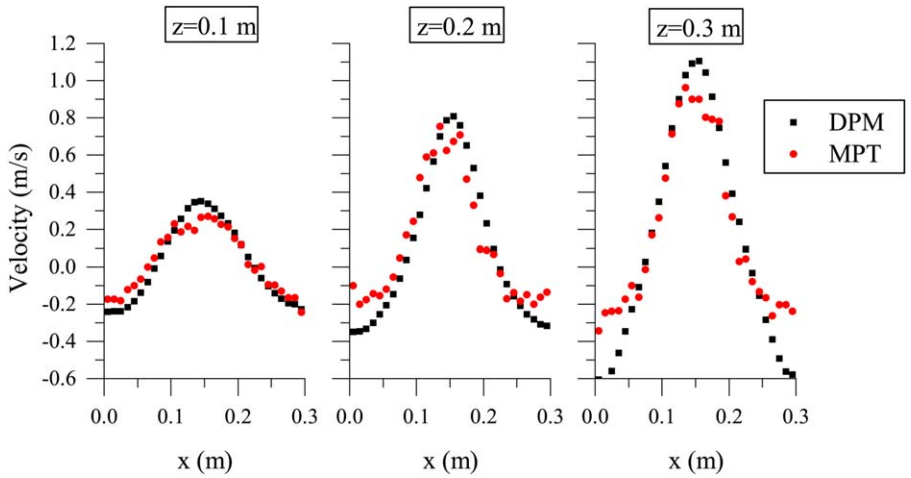

Figure 7. Comparison of the mean vertical velocity component (m/s) of the magnetic tracer particle and DPM bed material at different heights, $u_0 = 3.5$ m/s.

[Color figure can be viewed in the online issue, which is available at wileyonlinelibrary.com.]

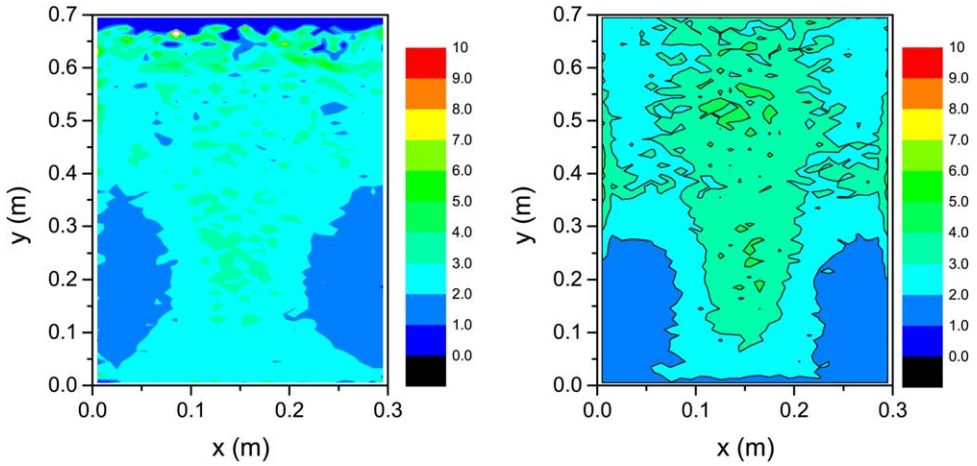

Figure 8. Contour plot of the mean rotational velocities (rot/s), for the MPT (left), and the DPM tracer particles (right).

[Color figure can be viewed in the online issue, which is available at wileyonlinelibrary.com.]

$$\varepsilon_s = \min\left(\frac{\frac{1}{6}\pi d_p^3 N_p}{V_{i,j}} \frac{O_{i,j}}{N_{\text{gridcells}}}, 0.6\right) \tag{25}$$

High superficial velocity u_0=3.5 m/s

Figure 6 shows the comparison of the solids fractions obtained from the MPT by using Eq. 25 and from the DPM. Figure 6 shows dense zones near the wall and a diluted area in the center where the bubbles pass. The qualitative comparison between the DPM and the MPT is very good. Similar bed expansion and solids fraction profiles can be seen. This shows that the hydrodynamic behavior is captured correctly by the model. Some differences in the shape of the dense zone are observed which might be related to the jump in the Ergun/Wen&Yu model at a porosity of 0.8.

For a contact in the sliding limit the particle rotation is dominated by the normal force, and thus for the translational velocity a quantitative comparison of the particle translation velocity is necessary to ensure a proper comparison of the rotational velocity. Figure 7 shows the vertical component of the (translational) velocity at three different cross sections inside the fluidized bed. Even though the MPT is slightly noisier, the two profiles are very similar, especially in the central region where the velocities are captured very well by the DPM. In the dense wall region, there is a deviation between the experiments and the model, which was also noticed by Van Buijtenen et al.[7] for a spouted bed. To correct for these effects Goniva et al.[8] added a rolling friction parameter ranging from 0 to 0.125 and found 0.125 to be the most appropriate based on the differences of translation velocity near the wall. In the simulation discussed in this article, the rolling friction was set to 0 and the friction coefficient to 0.1. For the left, right and bottom walls the friction parameter was set to a value of 0.3, because these are made of aluminum and stainless steel. The front and back plates are made of glass, which have a similar friction parameter as the bed material. An increase of the friction parameters led to a linear increase in the rotational velocity, indicating that the particle wall dynamics and the friction dominate the system. Instead the differences in the vertical velocity component near the wall can be explained by the limited depth of the system as compared to the particle diameter. Because the particle diameter is only 5 times smaller than the depth of the pseudo 2-D system difficulties in determining local porosity, drag, and particle bridging might affect

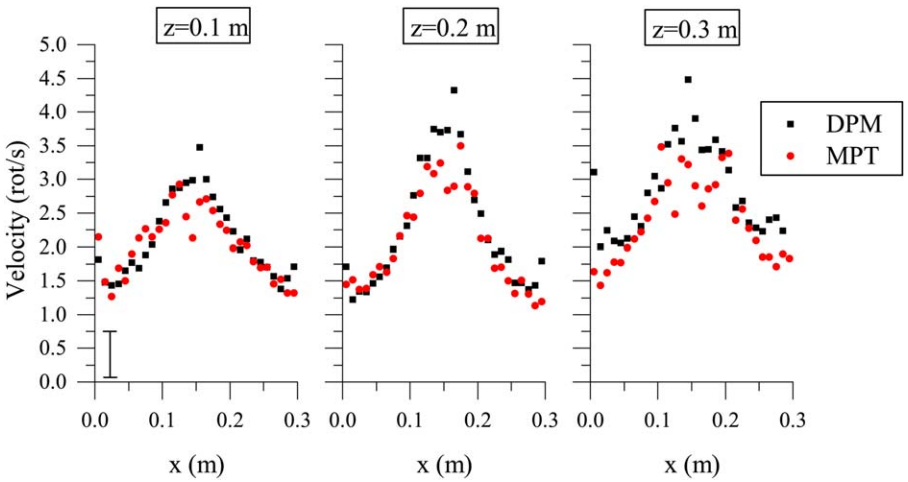

Figure 9. Mean rotational velocity (rot/s) comparison of magnetic tracer particle and DPM bed material at different heights, $u_0 = 3.5$ m/s.

[Color figure can be viewed in the online issue, which is available at wileyonlinelibrary.com.]

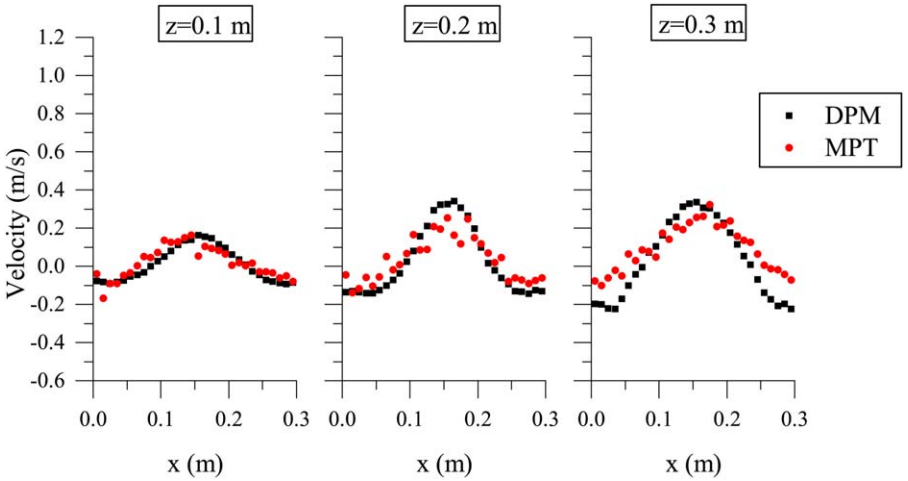

Figure 10. Mean vertical velocity component (m/s) comparison of magnetic tracer particle and DPM bed material at different heights, $u_0 = 2.5$ m/s.

[Color figure can be viewed in the online issue, which is available at wileyonlinelibrary.com.]

the hydrodynamic behavior. This might also explain the mismatch of the minimum fluidization velocity between the experiment and the simulation.

Now that the translational velocity is captured correctly the rotational velocity can be checked. Figure 8 shows a contour plot of the rotational velocity obtained from the MPT and the tracer particle in the DPM. The bed material in the model cannot be used for the rotational velocity because the inertial mass of the bed material does not match the tracer particle, which unfortunately is unavoidable. In both cases, an hourglass shaped profile can be seen which is expected. The MPT show some noise that is related to the limited number of data points. For the MPT, the results were obtained of tracking one magnet for 1 h, relating to 600 tracer in the DPM for 60 s in simulation time. In total about 200,000 datapoints were obtained. The spread in the rotational velocity is quite large and is related to the limited number of samples per grid cell, say $N \approx 200$. According to theory, an error of 0.7 rot/s is expected, following

$$\sigma_m = \frac{\sigma}{N} \tag{26}$$

The agreement with the DPM is remarkably good and to the best of the author's knowledge never shown before. The magnitude and overall profile of the rotational velocity both match very well. Again, near the wall and bottom region slight deviations can be seen, which can most probably be attributed to the mismatch of the translational velocity.

Figure 9 shows the rotational velocity at three different cross-sections in the fluidized bed with increments of 10 cm from the distributor plate. The magnitude of the rotational velocity matches very well and also the overall profile matches quite well. Near the wall region at a height of 0.3 m a slightly higher rotational velocity is found for the DPM, which can be directly related to the higher downwards translational velocity which is found in the DPM as can clearly be seen in Figure 7. The error bar in Figure 9 indicates the error in the measured rotational velocity, based on Eq. 26.

Low superficial velocity $u_0 = 2.5\,m/s$

The experiments in a pseudo 2-D fluidized bed setup were repeated at a lower superficial velocity of 2.5 m/s. Figures 10

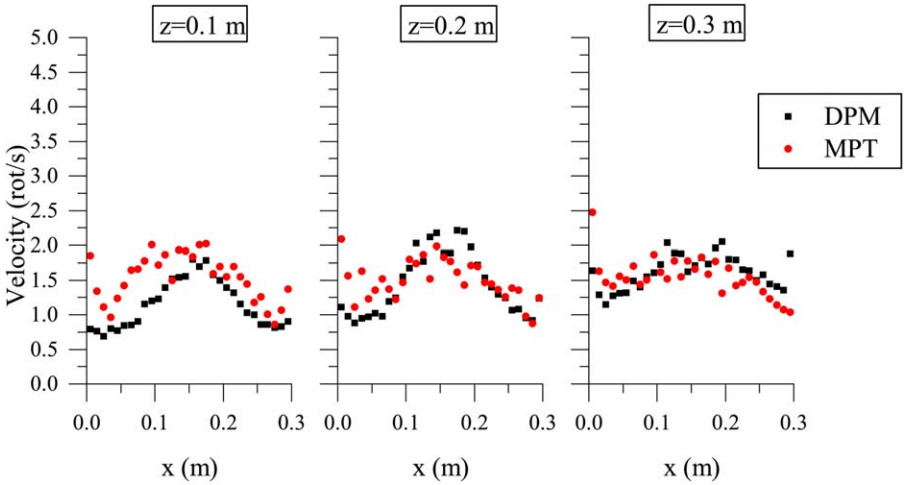

Figure 11. Mean rotational velocity (rot/s) comparison of magnetic tracer particle and DPM bed material at different heights, $u_0 = 2.5$ m/s.

[Color figure can be viewed in the online issue, which is available at wileyonlinelibrary.com.]

and 11 show the vertical velocity (m/s) and rotational velocity (rot/s) at a few cross-sections in the fluidized bed, respectively. Both the rotational and translation velocities are lower in comparison to Figures 7 and 9, respectively. This is expected because of the lower superficial velocity. The rotational velocity again matches fairly well. However, because the overall velocities are lower in comparison to Figure 9 the noise becomes more apparent. This can most clearly be seen at the lower section of the setup at 0.1 m.

Conclusions

For the first time, the particle rotational velocity in a gas fluidized bed was measured using a MPT method. It was shown that the error in the orientation of a magnetic marker has a linear dependency on the relative distance between the marker and the sensors and an inverse linear dependency on the magnetic strength. The magnetic particle acts as a compass to the earth's magnetic field even under fluidization conditions. This was compensated using a Helmholtz coil the operation of which was shown to be successful. An extensive comparison of the MPT technique with the DPM was made, showing a very good comparison. Both the solids fraction profile and particle translation velocity showed a very good comparison.

Finally, because the rotational velocity is measured as well, all aspects of the particle motion are now captured. This makes it possible to study the force balance on the particle in more detail; showing the particle rotation is dominated by the sliding regime. The use of a particle-wall friction parameter is key in getting the correct behavior. Only the bottom and side wall friction parameters deviate from the particle-particle friction parameter. The friction coefficient used to describe particle-wall friction for the front and back wall is the same as that used for particle–particle friction, because both involve glass-glass contacts. Rolling friction has been switched off in these simulations.

Addition of hydrodynamic torque, using an ad-hoc Richardson and Zaki[16] correction on the torque on a single sphere, has no noticeable effect for spherical particles. However a substantial effect is expected for nonspherical particles. MPT would be the ideal technique to quantify this effect.

Further research into the capabilities of the MPT technique includes the use of nonspherical particles, that is, rods. A clear difference on the rotational behavior is expected, especially related to the orientation of the particles to either the flow or the geometry of the system.

Acknowledgments

This research was funded by the European Research Council, under the Advanced Investigator Grant Scheme, contract no. 247298 (Multiscale flows), and the 3TU Centre of Excellence – Multiscale Phenomena.

Notation

Roman symbols

$\bar{H}$ = Magnetic field, A/m
Q = Quality function,
P = probability function,
S_t = Sensor signal, A/m
S_p = Source term, N/m^3
$\bar{F}$ = Force, N
V = Volume, m^3
$\bar{T}$ = Torque, N/m
I = Moment of intertia, kg m^2
C = Drag coefficient
Re = Reynolds number
O = Occupancy
R = Rolling friction parameter
p = pressure, N/m^2
$\bar{u}$ = velocity, m/s
u_0 = superficial velocity, m/s
$\bar{v}$ = velocity, m/s
m = mass, kg
k = spring stiffness, N/m
$\bar{e}$ = unit vector, -
t = time, s
t_{ab} = unit tangent vector
r = radius, m
$\bar{r}_p$ = position vector, m

Greek symbols

$\bar{\Omega}$ = relative tangential velocity, m/s
β = Drag coefficient
$\bar{\bar{\tau}}$ = stress, N/m^2
μ = Magnetic moment, Am^2
μ_f = viscosity, Pa s
μ_{fr} = friction parameter
μ_{rfr} = rolling friction parameter
ϵ_f = porosity
η = damping coefficient, kg/s
δ = overlap, m
θ = inclination angle
ϕ = azimuthal angle
$\bar{\omega}$ = rotational velocity, rot/s
ρ = density, kg/m^3
σ = standard deviation

Abbreviations and subscripts

MPT = Magnetic Particle Tracking
SQP = Sequential Quadratic Programming
DPM = Discrete Particle Modeling
x = in the x-direction
y = in the y-direction
z = in the z-direction
p = particle
ps = particle to sensor
s = solid
f = fluid
m = measured
t = theoretical or tangential
n = particle

Literature Cited

1. Wu X, Wang Q, Luo Z, Fang M, Cen K. Rotation speed measurement of moving particles in a cfb riser. *Particuology*. 2009;7(4): 238–244.
2. Phillips D, Lee M, Speirits F, Barnett S, Simpson S, Lavery M, Padgett M, Gibson G. Rotational doppler velocimetry to probe the angular velocity of spinning microparticles. *Phys Rev A*. 2014;90(1): 011801.
3. Yang Z, Fan X, Bakalis S, Parker D, Fryer P. A method for characterising solids translational and rotational motions using multiple-positron emission particle tracking (multiple-pept). *Int J Multiphase Flow*. 2008;34(12):1152–1160.
4. Buist KA, Gaag AC, Deen NG, and Kuipers JAM. Improved magnetic particle tracking technique in dense gas fluidized beds. *AIChE J*. 2014;60(9):3133–3142.
5. Neuwirth J, Antonyuk S, Heinrich S, Jacob M. CFD-DEM study and direct measurement of the granular flow in a rotor granulator. *Chem Eng Sci*. 2013;86:151–163.
6. Jajcevic D, Siegmann E, Radeke C, Khinast JG. Large-scale cfd–dem simulations of fluidized granular systems. *Chem Eng Sci*. 2013; 98:298–310.
7. Van Buijtenen MS, Börner M, Deen NG, Heinrich S, Antonyuk S, Kuipers JAM. An experimental study of the effect of collision properties on spout fluidized bed dynamics. *Powder Technol*. 2011; 206(1):139–148.

8. Goniva C, Kloss C, Deen NG, Kuipers JAM, Pirker S. Influence of rolling friction on single spout fluidized bed simulation. *Particuology*. 2012;10(5):582–591.
9. Deen N, Van Sint Annaland M, Van der Hoef M, Kuipers JAM. Review of discrete particle modeling of fluidized beds. *Chem Eng Sci*. 2007;62(1):28–44.
10. Ergun S. Fluid flow through packed columns. *Chem Eng Prog*. 1952;48:89–94.
11. Wen C, Yu Y. Mechanics of fluidization. *Chem. Eng. Prog. Symp. Ser*. 1966;62:100–111.
12. Cundall PA, Strack OD. A discrete numerical model for granular assemblies. *Geotechnique*. 1979;29(1):47–65.
13. Dennis S, Singh S, Ingham D. The steady flow due to a rotating sphere at low and moderate reynolds numbers. *J Fluid Mech*. 1980; 101(02):257–279.
14. Sawatzki O. Das strömungsfeld um eine rotierende kugel. *Acta Mechanica*. 1970;9(3–4):159–214.
15. Schiller L, Naumann Z. A drag coefficient correlation. *Vdi Zeitung*. 1935;77(318):51.
16. Richardson J, Zaki W. The sedimentation of a suspension of uniform spheres under conditions of viscous flow. *Chem Eng Sci*. 1954;3(2): 65–73.
17. Zastawny M, Mallouppas G, Zhao F, Van Wachem B. Derivation of drag and lift force and torque coefficients for non-spherical particles in flows. *Int J Multiphase Flow*. 2012;39:227–239.
18. Wildman R, Huntley J, Hansen JP, Parker D, Allen D. Single-particle motion in three-dimensional vibrofluidized granular beds. *Phys Rev E*. 2000;62(3):3826.

Manuscript received Mar. 13, 2015, and revision received June 17, 2015.